Sustainable Energy & Fuels

Photoelectrochemical water splitting using strain-balanced multiple quantum well photovoltaic cells

Journal:	*Sustainable Energy & Fuels*
Manuscript ID	SE-ART-05-2019-000276.R1
Article Type:	Paper
Date Submitted by the Author:	15-Jul-2019
Complete List of Authors:	Steiner, Myles; National Renewable Energy Laboratory Barraugh, Collin; National Renewable Energy Laboratory Aldridge, Chase; National Renewable Energy Laboratory Barraza Alvarez, Isabel; National Renewable Energy Laboratory; University of Texas at El Paso Ekins-Daukes, Nicholas; University of New South Wales Friedman, Daniel; National Renewable Energy Laboratory, Deutsch, Todd; National Renewable Energy Laboratory, Young, James; National Renewable Energy Laboratory,

Photoelectrochemical water splitting using strain-balanced multiple quantum well photovoltaic cells

Myles A. Steiner[1], Collin Barraugh[1], Chase Aldridge[1], Isabel Barraza Alvarez[1], Daniel J. Friedman[1], Nicholas J. Ekins-Daukes[2], Todd G. Deutsch[1], James L. Young[1]

1) National Renewable Energy Laboratory, Golden, CO 80401, United States
2) University of New South Wales, Sydney NSW2052, Australia

Abstract

Starting from the classical GaInP/GaAs tandem photoelectrochemical water splitting device, higher solar-to-hydrogen efficiencies can be pursued by extending photon absorption to longer wavelengths. We incorporate strain-balanced GaInAs/GaAsP quantum wells into the bottom GaAs junction, to increase the range of photon absorption. The inclusion of 1.34 eV quantum wells in the depletion region of the bottom cell extends the absorption edge to 930 nm. With a corresponding increase in the thickness of the top cell for current matching, the light-limiting photocurrent increases by >8%. The estimated solar-to-hydrogen efficiency is 13.6 ± 0.5 %, and we show a pathway to further improvement. With the semiconductor device remaining on the growth substrate, this quantum well architecture may enable improved stability and durability of the photoelectrochemical electrodes.

INTRODUCTION

Photoelectrochemical (PEC) water splitting is a potentially sustainable process for generating hydrogen gas that can be stored efficiently and converted back to usable electricity in a fuel cell. Solar-to-hydrogen (STH) efficiencies in the range of 10-12% have been demonstrated over the past twenty years using GaInP/GaAs dual junction photovoltaic-based tandem PEC devices immersed in electrolyte (1). With junction bandgaps of ~1.82 and 1.42 eV, respectively, these baseline devices generate sufficient voltage to overcome the 1.23 V thermodynamic potential as well as an additional ~0.5 V of electrochemical half-reaction kinetic overpotentials. With good surface co-catalysts to minimize the kinetic overpotentials of the hydrogen evolution and oxygen evolution reactions (HER and OER), the GaInP/GaAs device generates an oversupply of photovoltage that is ultimately unused. The STH efficiency is proportional to the generated photocurrent, and only photons above the two junctions' bandgaps can be absorbed. Since a lower bandgap device can generate a higher photocurrent at the cost of generating lower voltage, an ideally designed device would have bandgaps that generate just enough voltage to split water. Doescher *et al.* showed the ideal bandgap combination to be approximately as low as 1.7/1.1 eV (2).

Progress toward higher STH efficiency was demonstrated at NREL by using a so-called "inverted metamorphic multijunction" (IMM) architecture (3), changing the lattice constant of the bottom cell in order to access a lower bandgap alloy for the bottom junction. GaInP/GaInAs devices with junction bandgaps of 1.8 eV and ~1.2 eV demonstrated STH efficiencies >16% (4), and preliminary data indicated that a 1.7/1.1 eV tandem might be feasible. In fabricating an IMM

device, the epitaxial films are removed from the growth substrate and bonded to a secondary mechanical handle.

By contrast, the traditional, on-substrate GaInP/GaAs architecture, although limited to lower practical STH efficiencies, nonetheless has advantages in terms of stability, durability and processability that may be more important for a working PEC device than STH efficiency. Some co-catalysts, for example, are deposited at close to 500°C which would be much more challenging with an IMM device (5).

Here we show that a GaInP/GaAs device can be improved significantly by including multiple quantum wells (QWs) and a Bragg reflector in the bottom cell, in order to extend the wavelength range of photon absorption. Quantum wells are composed of a low-bandgap well layer that is surrounded by high-bandgap barrier layers. Multiple repeating units of this basic barrier/well/barrier structure increase the total absorption in the well, and the Bragg reflector increases the optical pathlength through the QWs (6). By adding strain-balanced GaAsP/GaInAs QWs in the depleted region of the GaAs bottom junction, the absorption range is extended from ~870 nm to ~930 nm (7), leading to an overall increase of >2 mA/cm^2 that is split between the two cells, or equivalently a gain of >1 mA/cm^2 in the light-limiting photocurrent of a current-balanced tandem. This represents a >8% increase in the relative STH efficiency compared to a baseline GaInP/GaAs device. Since the baseline device has an oversupply of voltage, the ~100 mV drop in voltage because of the QWs does not adversely affect the STH efficiency. With an optimized structure, the relative increase in STH efficiency could exceed 10%.

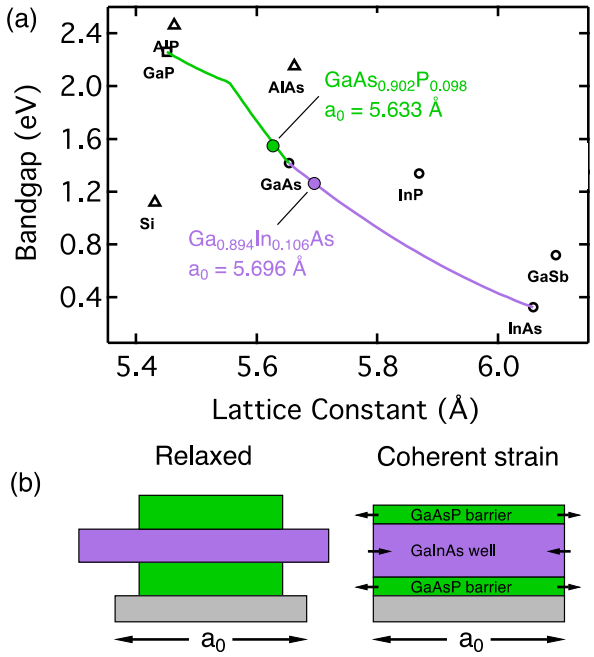

Figure 1 (a) Bandgap and lattice constant of common III-V binary and ternary alloys. The alloys used in the QWs, along with their relaxed lattice constants, are indicated. (b) Relationship between relaxed and coherently-strained layers. The GaInAs layers are compressively strained, the GaAsP layers are tensile strained. The sizes are exaggerated for clarity.

Quantum wells have been developed for other optoelectronic applications including photovoltaics and detectors (7-11), and have been incorporated into GaInP, GaAs and InP devices.

Here we briefly review the important features of quantum well PV devices; the reader is referred to the literature (12, 13) for more details and references.

To extend the absorption edge of a GaAs solar cell, we use strain-balanced QWs composed of GaInAs wells and GaAsP barriers. As shown in Fig. 1a, neither of these families of ternary alloys are lattice-matched to the GaAs substrate, and thus care must be taken to fabricate the device so as not to develop a significant density of deleterious structural dislocations (14). A lattice-mismatched material can be grown coherently strained, with the same in-plane lattice constant as the substrate but a strained out-of-plane lattice constant, up to a critical thickness at which deleterious dislocations form and the material relaxes. Figure 1b illustrates the structural effect of coherently straining the two layers to the substrate lattice constant. The compressive strain in the GaInAs well leads to a larger out-of-plane lattice constant, whereas the tensile strain in the GaAsP leads to a smaller out-of-plane lattice constant.

The carrier collection in the quasi-neutral region of a planar pn-junction solar cell is dominated by diffusion of minority carriers. In the QW region, however, the strong spatially-varying potential reduces the diffusion length to nearly zero. The QWs are therefore situated in the depletion region between the two quasi-neutral regions, shown in Fig. 2a, and carrier collection in this region is dominated by thermal excitation of carriers out of the wells followed by drift in the electric field (15, 16). Tunneling of carriers between adjacent wells is also possible if the barriers are thin enough, though with 170 Å barriers the tunneling probability is nearly zero for these QWs.

The cells used in this work were composed of ~170 Å $GaAs_{0.902}P_{0.098}$ barriers with a relaxed bandgap of ~1.53 eV, and ~85 Å wells $Ga_{0.894}In_{0.106}As$ with a bandgap of ~1.27 eV. The layer thicknesses were chosen so that the net strain (or stress) in the full structure was zero at the growth temperature (14), but the individual layers are still coherently strained. The actual absorption edge of the QW is determined by a combination of that elastic strain and two-dimensional quantum confinement in the direction perpendicular to the barrier-well interfaces. The quantum-confined Stark effect due to the net electric field can lead to small additional shifts in the absorption edge. In the GaInAs well, compressive strain raises the energy of the conduction and heavy hole bands and lowers the energy of the light hole band, leading to the dominant optical transition between the conduction and heavy hole bands (9). In the GaAsP barriers, tensile strain has the opposite effect, lowering the energy of the conduction and heavy hole bands and raising the energy of the light hole band, leading to the dominant optical transition between the conduction and light hole bands. Following the methodology of (9), the strained barrier and well materials have calculated bandgaps of ~1.49 eV and ~1.31 eV, respectively. The remainder of the energy shift up to ~1.34 eV comes from the two-dimensional quantum confinement. Using standard values of the elastic constants and band offsets, interpolated to the specific compositions of GaInAs and GaAsP, we calculate the well depth to be 151 mV in the conduction band and 28 mV in the heavy hole band (9). This strong asymmetry is illustrated in Figure 2b.

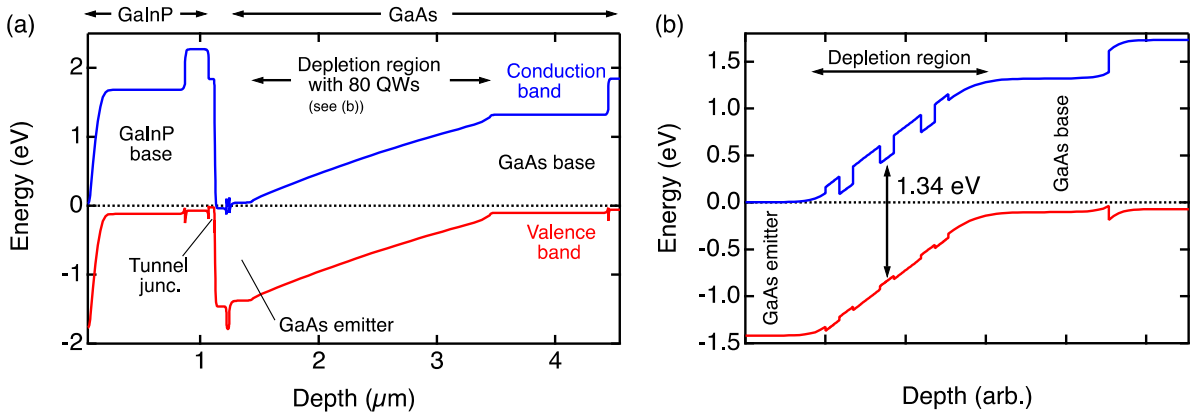

Figure 2 (a) Equilibrium band diagram of the device, and (b) the depletion region of the bottom cell. The horizontal axis in (a) accurately represents the tandem device, whereas the horizontal axis in (b) is notional and the diagram shows only three QWs for clarity. Most of the band offset in the QWs is in the conduction band.

It is essential that the background doping in the QW region be low so that the QW region can be as wide as possible in order to maximize photon absorption. For a background doping of ~1x10^{14}/cm^3 in GaAs, the depletion region is ~2 μm wide. Using QWs with 85 Å wells and 170 Å barriers, a maximum of ~80 QWs can fit in the depletion region. Since only 1/3 of the volume is made of well material, the cumulative thickness of the wells in the QW region is ~0.7 μm, lower than the optical thickness of a few microns for GaAs-like semiconductors.

The optical pathlength can be nearly doubled by adding a reflector behind the bottom cell. In principle the gold back contact could serve as a reflector, if the substrate were to be polished on both sides, though parasitic sub-bandgap absorption because of the long Urbach tail in GaAs could reduce the reflectance. Another solution is to grow an alternating sequence of high- and low-index layers to form a narrow band Bragg reflector. These kinds of structures are widely used in solid state lasers, with reflectance >99%. Here we used 20 sets of AlAs/GaAs with the individual thicknesses tuned to give a peak reflectance at 920 nm, corresponding to the absorption edge of the QWs.

EXPERIMENTAL DETAILS

The devices reported here were grown by atmospheric pressure metalorganic vapor phase epitaxy (MOVPE) on a custom-built reactor. Metalorganic sources included triethylgallium, trimethylgallium, trimethylindium and trimethylaluminum for group-III elements, arsine and phosphine for group-V elements, diethylzinc and carbon tetrachloride for the p-type dopants zinc and carbon, and disilane and hydrogen selenide for the n-type dopants silicon and selenium. Semiconductor material was deposited on an (001) GaAs substrate, miscut 4° toward the <111>B to maximize the kinetic CuPt ordering in the GaInP alloy. The bandgap of GaInP can vary from 1.8 eV (ordered) to 1.9 eV (disordered), so the lower bandgap ordered alloy leads to increased photocurrent generation in the top junction. Additional growth details are provided in the ESI.

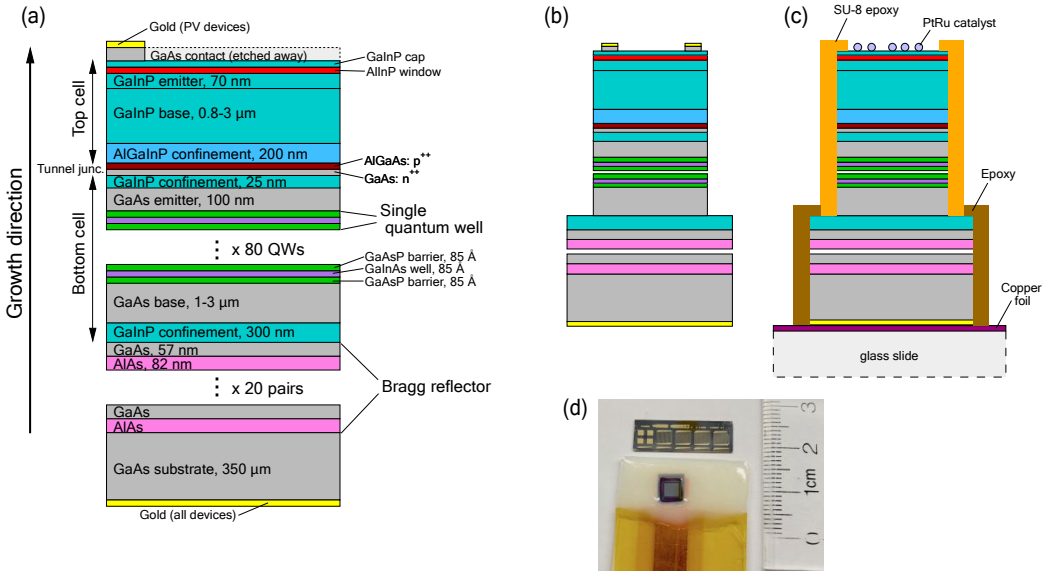

Figure 3 (a) Schematic of the tandem solar cell, including the QW region and a 20-layer Bragg reflector. Some cells in this work exclude one or both of those layer sets. Schematic is not to scale. (b) isolated PV device with front contacts. (c) isolated PEC electrode, with SU-8 isolating the mesa, epoxy protecting the cleaved sidewalls, and copper foil electrical contact to the back. (d) photographs of PV and PEC devices. The PV sample shows 4 cells and a Hall bar; the PEC sample shows a single device.

The devices were grown upright, starting from the GaAs bottom cell at 650°C, followed by an AlGaAs/GaAs tunnel junction at 600°C and finally the GaInP top cell at 700°C. The top cell included a thin AlInP window layer to passivate the emitter, and a thin GaInP cap layer to protect the AlInP window from etching in the electrolyte. The growth also included a heavily doped front contact layer for aid in making test structures, that was later removed to make PEC devices. For cells that included quantum wells, an AlAs/GaAs Bragg reflector was grown below the bottom cell, and the GaInP top cell was thickened to ~3 µm to current-match the two cells.

The GaAs cell thickness was nominally 3 µm in all cases: with no QWs the GaAs base layer was 3 µm, whereas in the cells with a 2-µm intrinsic region that contained 80 QWs, the GaAs base layer was thinned to 1 µm. A schematic of the full device is shown in Figure 3, including additional cladding layers to improve minority carrier confinement and transport.

After growth, a portion of the material was cleaved off for photovoltaic (PV) test devices, while the remainder was used for PEC electrodes. All processing was carried out in a class 1000 cleanroom using standard photolithographic and wet-chemical etching techniques. For both sets of devices, gold was electroplated to the substrate to form a back electrical contact. For the PV devices, gold front contacts were electroplated through a positive photoresist mask and individual devices were isolated. The devices had mesa areas of 11.6 mm^2 and illuminated areas of 10.0 mm^2.

For the PEC electrodes, the front contact layer was etched away. Individual devices were isolated and the sidewalls were protected with SU-8 2002 transparent dielectric epoxy. The exposed surface of the isolated mesas were "flash" sputtered with a PtRu catalyst for 3 seconds at 20 watts in a 10 mTorr UHP argon background. This deposition yielded 2-5 nm PtRu particles covering a fraction of the semiconductor surface and total PtRu loading of approximately 500 ng/cm^2 (4). The PEC devices had a nominal front area of 11.6 mm^2. Further details about the electrode fabrication are provided in the ESI.

For the PV measurements, external quantum efficiency was measured on custom-built and calibrated instrumentation based on a tungsten-halogen lamp and a 270m monochromator, and SR830 dual-channel lock-in amplifiers. The data resolution was 5 nm. High brightness Mightex LEDs peaking at 470 nm and 850 nm were used to light-bias the devices, to observe the characteristics of the individual junctions. Current-voltage measurements were taken on a solar simulator with a xenon lamp and high brightness LEDs to shape the spectrum. The intensity was set using calibrated GaInP and GaAs reference cells and the spectrum was measured with a Spectral Evolution high speed spectrophotometer.

For PEC measurements, the incident photon-to-current efficiency (IPCE) was measured with 10 nm FWHM resolution in a three-electrode configuration using the solar cell as the working electrode, a mercury/mercurous sulfate reference electrode (MSE) with 0.5 M sulfuric acid filling solution, and a platinum flag counter electrode. The electrodes were submerged in a glass cell containing 0.5 M sulfuric acid with 1 mM Triton X-100 surfactant. Light from a Xe arc lamp was passed through an Acton Research SP-50 monochromator and focused onto the middle of the device in an "underfill" configuration to mitigate any uncertainty in active surface area. Before obtaining measurements, the monochromated output was measured using a calibrated photodiode. Light biases of 808 nm or 532 nm were applied when measuring the top or bottom cell response, respectively.

Two-electrode PEC current-voltage (JV) measurements were performed with an IrO_x-coated Ti mesh (Water Star Inc.) counter electrode and 0.5 M sulfuric acid electrolyte with 1 mM Triton X-100 surfactant added. The illumination from an ABET Technologies Sun 3000 solar simulator was set using calibrated GaInP and GaAs reference cells for top-limited and bottom-limited devices, respectively. Because of refraction through the glass window of the sample holder, we estimate the light to be concentrated to ~1.1X, so that the measured photocurrents are systematically inflated relative to the reference spectrum. We will estimate the absolute STH efficiency from the IPCE data, as described below.

RESULTS AND DISCUSSION

Figure 4a shows the EQE for a preliminary set of single junction GaAs PV cells with different numbers of GaInAs/GaAsP quantum wells. These cells were fabricated to calibrate the QWs and Bragg reflector, but no PEC electrodes were made. Compared to the baseline cell with no QWs, the absorption edge for all cells with QWs is shifted to 930 nm, and an exciton peak can be clearly observed. The plateau at ~900 nm increases from ~21% to ~36% as the number of QWs is increased from 50 to 95. Figure 4b illustrates the effect of a Bragg reflector on a GaAs cell with 80 QWs. The red dashed line shows the reflectance as measured directly on the Bragg reflector, clearly centered over the QW region. As shown in the red solid line, the presence of the reflector creates interference between forward- and backward-travelling waves, making the plateau difficult to discern. Those interference fringes can be smoothed out with an anti-reflection coating, shown in purple. Comparing the blue and purple curves, the EQE increase by ~1.34X at short wavelengths due to the ARC, but by ~2.14X at 900 nm due to the ARC and the Bragg reflector, from which we can nominally deduce a ~1.6X increase in the QW absorption due to the Bragg reflector.

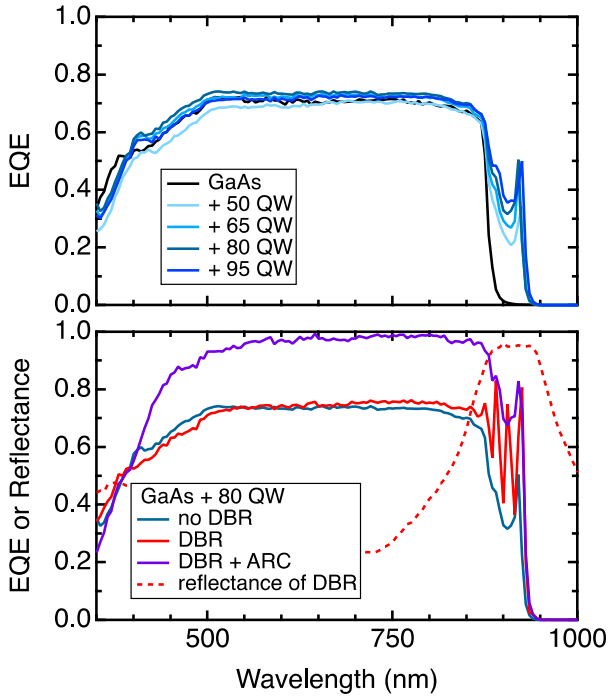

Figure 4 External quantum efficiency of single junction GaAs cells with strain-balanced GaInAs/GaAsP quantum wells. (a) Different number of QWs, as indicated. (b) Cells with 80 QWs, with a Bragg reflector and ARC. The dashed line shows the reflectance of the Bragg reflector as measured after etching away the cell layers above it.

Several tandem devices were grown and characterized, as indicated in Table 1. EQE and IPCE data are shown in Figure 5 for one sample of each device. JV and PEC data are shown in Figure 6 for the one sample of each device, with additional data provided in the ESI.

Table 1 Device

Device	Top cell	Bottom cell	Color	PV		PEC		Device ID
				Jsc (mA/cm²)	Voc (V)	Jsc (mA/cm²)	V(0.99 x Jsc)	
Baseline	1-µm GaInP	GaAs	Black	9.34	2.354	12.1	+0.075	MR555
Cntrl1	1-µm GaInP	GaAs+QW+Bragg	Light blue	9.68	2.305	12.4	+0.065	MR635
Cntrl2	3-µm GaInP	GaAs	Dark blue	8.83	2.325	11.1	>0	MR657
QW1	3-µm GaInP	GaAs+QW+Bragg	Red	10.48	2.327	13.1	+0.088	MR706

The baseline device, shown in black, is a nominally current-matched GaInP/GaAs tandem with a ~0.8 µm top cell and a 3 µm bottom cell. This tandem did not include a Bragg reflector because the 3-µm GaAs was already optically thick. Integrating the IPCE curves over the AM1.5 direct solar spectrum indicates that the tandem is, in fact, slightly bottom-limited.

Adding quantum wells and a Bragg reflector to the bottom cell (light blue) shifts the absorption edge to 930 nm which in turn increases the photogenerated current in the bottom cell. The response of the top cell remains the same, as shown in the EQE and IPCE curves, but the increased current in the bottom cell now makes the device top-limited. Because the baseline was slightly bottom-limited the overall short-circuit current increases slightly, as shown in both sets of

JV curves. Figure 6a shows that the open-circuit voltage (Voc) has dropped by ~70 mV, corresponding to the shift in absorption edge due to the incorporation of QWs. The cell still exhibits the light-limiting photocurrent at zero volts.

The control cell in dark blue had a 3-µm top cell but only a GaAs bottom cell. Figure 5 shows an increase in the long wavelength EQE and IPCE response of the top cell, because of the increased thickness. In this configuration the tandem is now severely bottom-limited, and the short-circuit current drops compared to the baseline device. The Voc of this GaInP/GaAs cell is largely unchanged from the baseline because the bandgaps have not changed; the changes in generated photocurrent in the two cells have only logarithmic effects on the Voc.

Finally, the red curve shows a device MR706 with a 3-µm top cell, 80 QWs in the bottom cell, and a Bragg reflector. The cell shows the increased absorption range due to the QWs, as well as the increased response in the top cell. With increased photoresponse in both junctions, the short-circuit current of device MR706 has increased by 1.0 mA/cm^2 compared to the baseline. This increase corresponds to a relative increase in STH efficiency of >8%.

Figure 7 shows the photocurrents extracted from the full set of electrodes; data are included in the ESI. The first three sample sets showed good catalytic effects and a light-limiting photocurrent at 0V, whereas the last sample set showed marginal behavior at 0V. Thus the photocurrent at -0.5 V was also included, to represent the potential performance with a slightly better co-catalyst. Focusing on the blue data points, the QW cell exhibits a 9.8% improvement in photocurrent compared to the baseline cell.

For completeness, we can also estimate the absolute efficiency of our best device. With the thermodynamic water-splitting potential at 25 °C being 1.23 V, STH efficiency is directly proportional to the current density at short circuit J_{sc} and defined as:

$$STH = \left[\frac{\left| J_{sc}\left(\frac{mA}{cm^2}\right) \right| \times (1.23\ V) \times \eta_F}{P_{total}\left(\frac{mW}{cm^2}\right)} \right]_{AM\ 1.5G} \qquad (1).$$

The AM1.5 global solar reference spectrum has total power P_{total} = 100 mW/cm^2. The Faradaic efficiency η_F is assumed to be equal to 100%, which is reasonable considering previous demonstrations for similar devices (1, 17). The light-limited photocurrent can be estimated by integrating the IPCE over the global spectrum, and previously we have shown good agreement between that estimate and rigorous outdoor on-sun benchmarking measurements (4). For the red data in Figure 5, the estimated photocurrents are 12.38 and 11.03 mA/cm^2 for the top and bottom cells, respectively, and the limiting current leads to an STH efficiency of 13.6 ± 0.5%. The estimated uncertainty is dominated by the standard deviation in measured photocurrents for the quantum well electrodes. With slightly improved collection efficiency in the QW region and optimized current matching, the STH could increase to 11.94 x 1.23 = 14.7%.

To evaluate whether the introduction of MQWs influences device stability during operation, we compare durability test data of otherwise equivalent samples with and without MQWs. These tests (Figure S3) were performed under constant illumination and unassisted water splitting conditions (i.e. two-electrode, short-circuit configuration) vs. an IrO_x counter electrode. Both device types show similar behavior with an initial 2-hr period of relatively good photocurrent stability followed by approximately linear decline over the next 8-10 hours that corresponds to a degradation rate of about 1.5 mA/cm^2 per hour. These results are similar to previous stability

reports (4, 17) for high-efficiency III-V PEC devices using platinum-group metal co-catalyst without additional corrosion protection strategies. These stability results show that the efficiency gains from introducing MQWs were achieved while maintaining a similar baseline level of device durability.

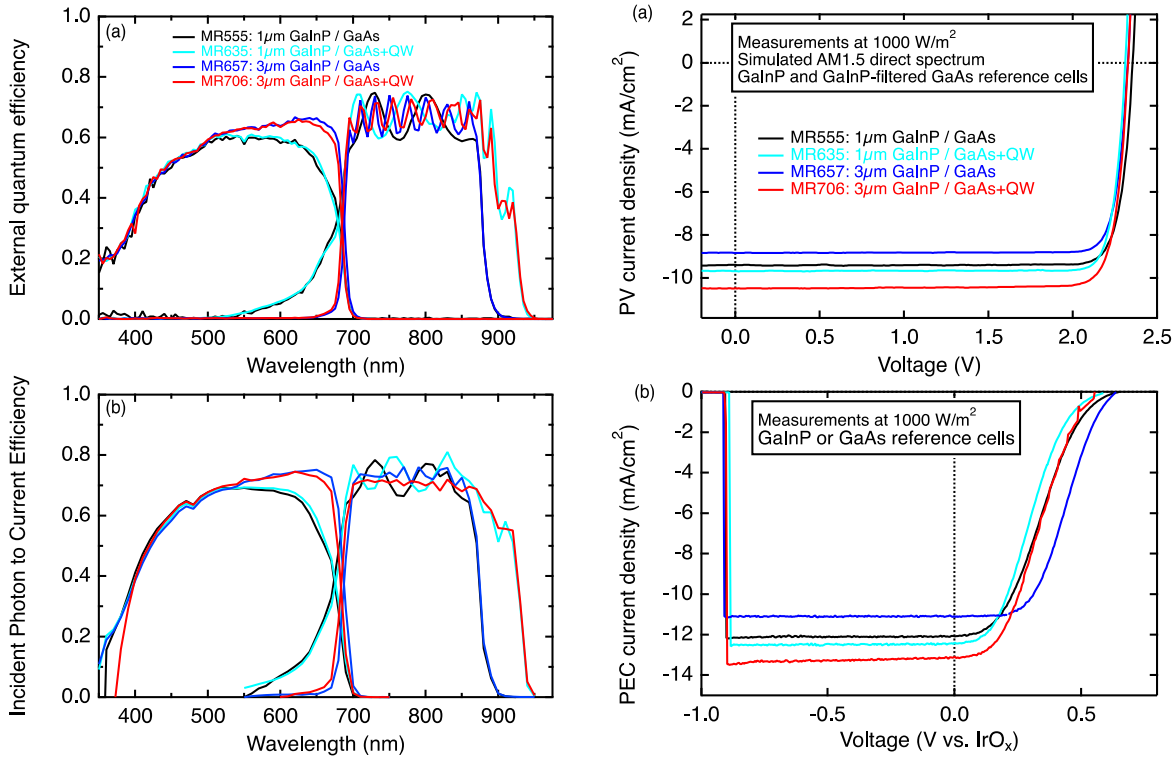

Figure 5 (a) EQE of PV devices, and (b) IPCE of PEC devices. The color code is the same for both graphs. The IPCE data appear slightly higher than the EQE because the aqueous electrolyte acts as an anti-reflection layer.

Figure 6 Current-voltage curves for (a) PV and (b) PEC devices. The PEC devices were measured in 0.5M sulfuric acid, with respect to an iridium oxide counter electrode. For both data sets, the intensity was set to 1000 W/m^2 to simulate the AM1.5 reference spectrum. Some light is collimated in the PEC measurement, effectively increasing the concentration.

For PV electricity generation applications, the absorption edge is ideally extended out to 930 nm which corresponds to the edge of a broad water-absorption dip in the global spectrum. Extending to slightly longer wavelengths comes at the expense of a further drop in voltage but without a significant increase in photocurrent, and since the PV efficiency depends on both current and voltage, it is not beneficial to extend the absorption beyond 930 nm. For PEC applications, however, only the photocurrent is important, provided that sufficient voltage still exists to split water. Thus, in principle, the QW architecture can be used to extend the absorption range to even longer wavelengths beyond 1000 nm where the water absorption band ends.

There are three main challenges to extending the absorption range beyond 930 nm. First, though the overall QW region is strain-balanced, the individual layers are coherently strained, and there is a maximum thickness that a strained layer can be grown before it relaxes. Such relaxation is mediated by the creation of misfit and threading dislocations that degrade the material quality.

Extending the absorption edge to longer wavelengths requires either significantly thicker wells, or a more indium-rich GaInAs alloy that in turn means more strain for a given thickness.

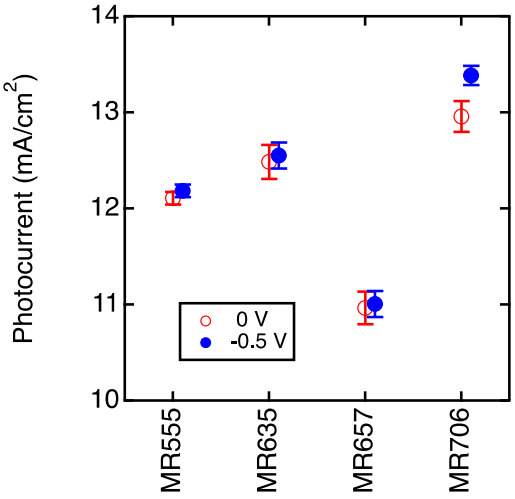

Figure 7 Short-circuit photocurrent of the four devices, at 0 V (red) and -0.5 V (blue) relative to an IrO_x counter electrode. The actual JV curves are shown in the ESI. Only curves that exhibited the light-limited photocurrent at 0 V were included in the analysis. The error bars indicate the standard deviation.

Second, GaInP is optically thick at ~3 μm, meaning that it absorbs nearly all of the incident light above its bandgap. As exemplified by the light-blue control cell in Figure 6a, increasing the bottom cell absorption without a corresponding increase in the top cell absorption does not lead to a boost in STH efficiency, since the tandem device is now top cell-limited. Further increases in the top cell photocurrent necessitate a lower bandgap, likely by growing GaInAsP or AlGaAs (18) rather than GaInP. As shown by Jain *et al*. (19, 20) GaInAsP is possible but the quaternary alloy is prone to immiscibility, phase separation and reactor calibration drift that make it considerably more difficult to fabricate. GaInAsP/GaInP quantum wells in the GaInP top cell can also be used to extend the absorption edge (21-23).

Third, the reduction in voltage due to the shifted absorption edge can be neglected only insofar as the tandem device still has sufficient voltage to split water at the light-limiting photocurrent. Whether that is true depends in part on the efficacy of the co-catalyst. The red JV curve in Figure 6b exhibits an elbow just above zero volts, with little voltage to spare. Reduced overpotential losses could come from advanced co-catalysts that are deposited at very high temperatures (5, 24, 25). Deposition at high temperature is largely enabled by maintaining the original form factor of an on-substrate PEC tandem.

In summary, we have shown that the efficiency of GaInP/GaAs tandem cells for photoelectrochemical water splitting can be significantly enhanced through the incorporation of strain-balanced quantum wells to extend the absorption edge out to 930 nm. The solar-to-hydrogen conversion efficiency increases by ~8% relative to the baseline, with a pathway to additional increases by further extending the absorption edge and lowering the top cell bandgap.

CONFLICTS OF INTEREST

There are no conflicts to declare.

ACKNOWLEDGMENTS

The authors are very pleased to thank J. Simon, H. Doescher, R. Mow and W. Callahan for useful conversations, and W. Olavarria for technical work. This work was authored by the National Renewable Energy Laboratory, operated by Alliance for Sustainable Energy, LLC, for the U.S. Department of Energy (DOE) under Contract No. DE-AC36-08GO28308. Funding provided by U.S. Department of Energy, Office of Energy Efficiency and Renewable Energy, Fuel Cell Technologies Office. The views expressed in the article do not necessarily represent the views of the DOE or the U.S. Government. The U.S. Government retains and the publisher, by accepting the article for publication, acknowledges that the U.S. Government retains a nonexclusive, paid-up, irrevocable, worldwide license to publish or reproduce the published form of this work, or allow others to do so, for U.S. Government purposes.

References

1. Turner JA, Khaselev O. A monolithic photovoltaic-photoelectrochemical device for hydrogen production via water splitting. Science. 1998;280(5362):425.
2. Doscher H, Geisz JF, Deutsch TG, Turner JA. Sunlight absorption in water - efficiency and design implications for photoelectrochemical devices. Energy & Environmental Science. 2014;7(9):2951-6.
3. Friedman DJ, Deutsch T, Turner J, Doescher H, Young J, Steiner MA, et al., inventorsDevices And Methods For Photoelectrochemical Water Splitting patent 10,087,535 B2. 2018.
4. Young JL, Steiner MA, Doescher H, France RM, Turner JA, Deutsch TG. Direct solar-to-hydrogen conversion via inverted metamorphic multi-junction semiconductor architectures. Nature Energy. 2017;2:17028.
5. Calvinho KUD, Laursen AB, Yap KMK, Goetjen TA, Hwang S, Murali N, et al. Selective CO2 reduction to C3 and C4 oxyhydrocarbons on nickel phosphides at overpotentials as low as 10 mV. Energy Environ Sci. 2018;11:2550-9.
6. Bushnell DB, EkinsDaukes NJ, Barnham KWJ, Connolly JP, Roberts JS, Hill G, et al. Short-circuit current enhancement in Bragg stack multi-quantum-well solar cells for multi-junction space cell applications. Solar Energ Mater Solar Cells. 2003;75(1-2):299-305.
7. EkinsDaukes NJ, Barnham KWJ, Connolly JP, Roberts JS, Clark JC, Hill G, et al. Strain-balanced GaAsP/InGaAs quantum well solar cells. Appl Phys Lett. 1999;75(26):4195-7.
8. Adams JGJ, Browne BC, Ballard IM, Connolly JP, Chan NLA, Ioannides A, et al. Recent results for single-junction and tandem quantum well solar cells. Progress in Photovoltaics: Research and Applications. 2011;19(7):865-77.
9. Zhang Y, Ning Y, Zhang L, Zhang J, Zhang J, Wang Z, et al. Design and comparison of GaAs, GaAsP and InGaAlAs quantum-well active regions for 808-nm VCSELs. Opt Express. 2011;19(13):12569.
10. Bradshaw GK, Samberg JP, Carlin CZ, Colter PC, Edmondson KM, Hong W, et al. GaInP/GaAs Tandem Solar Cells With InGaAs/GaAsP Multiple Quantum Wells. J Photovoltaics. 2014;4:614.
11. Sugiyama M, Wang Y, Fujii H, Sodabanlu H, Watanabe K, Nakano Y. A quantum-well superlattice solar cell for enhanced current output and minimized drop in open-circuit voltage under sunlight concentration. J Phys D: Appl Phys. 2013;43:024001.
12. Sayed I, Bedair SM. Quantum Well Solar Cells: Principles, Recent Progress, and Potential. J Photovoltaics. 2019;9(2):402-23.
13. Nelson J. Electronic states and optical properties of quantum wells. In: Barnham K, Vvedensky D, editors. Low-dimensional semiconductor structures. Cambridge: Cambridge University Press; 2001.
14. Ekins-Daukes NJ, Kawaguchi K, Zhang J. Strain-Balanced Criteria for Multiple Quantum Well Structures and Its Signature in X-ray Rocking Curves. Crystal Growth and Design. 2002;2(4):287-92.
15. Carlin CZ, Bradshaw GK, Samberg JP, Colter PC, Bedair SM. Minority Carrier Transport and Their Lifetime in InGaAs/GaAsP Multiple Quantum Well Structures. IEEE Trans Electron Devices. 2013;60(8):2532.

16. Nelson J, Paxman M, Barnham KWJ, Roberts JS, Button C. Steady-State Carrier Escape from Single Quantum Wells. IEEE Journal of Quantum Electronics. 1993;29(6):1460.
17. May MM, Lewerenz H-J, Lackner D, F.Dimroth, Hannapel T. Efficient direct solar-to-hydrogen conversion by in-situ interface transformation of a tandem structure. Nat Commun. 2015;6:8286.
18. Heckelmann S, Lackner D, Karcher C, Dimroth F, Bett AW. Investigations on AlxGa1-xAs solar cells grown by MOVPE. IEEE Journal of Photovoltaics. 2015;5(1):446-53.
19. Jain N, Geisz JF, France RM, Norman AG, Steiner MA. Enhanced current collection in 1.7 eV GaInAsP solar cells grown on GaAs by metalorganic vapor phase epitaxy. J Photovoltaics. 2017;7(3):927-33.
20. Jain N, Schulte KL, Geisz JF, Friedman DJ, France RM, Perl EE, et al. High-efficiency inverted metamorphic 1.7/1.1 eV GaInAsP/GaInAs dual-junction solar cells. Appl Phys Lett. 2018;112:053905.
21. Sayed IEH, N.Jain, Steiner MA, Geisz JF, Bedair SA. 100 period InGaAsP/InGaP Superlattice Solar Cell with Sub-bandgap Quantum Efficiency Approaching 80%. Appl Phys Lett. 2017;111:082107.
22. Lee K-H, Barnham KWJ, Connolly JP, Browne BC, Airey R, Roberts JS, et al. Demonstration of photon coupling in dual multiple-quantum-well solar cells. IEEE Journal of Photovoltaics. 2012;2(1):68-74.
23. Lee K-H, Barnham KWJ, Roberts JS, Alonso-Alvarez D, Hylton NP, Fuhrer M, et al. Investigation of carrier recombination dynamics of InGaP/InGaAsP multiple quantum wells for solar cells via photoluminescence. J Photovoltaics. 2017;7(3):817-21.
24. Porter SH, Hwang S, Amarasinghe V, Taghaddos E, Manichev V, Li M, et al. Optimizing “Artificial Leaf” Photoanode-Photocathode-Catalyst Interface Systems for Solar Water Splitting. ECS Transactions. 2016;72(37):1-19.
25. Britto RJ, Benck JD, Young JL, Hahn C, Deutsch TG, Jaramillo TF. Molybdenum Disulfide as a Protection Layer and Catalyst for Gallium Indium Phosphide Solar Water Splitting Photocathodes. J Phys Chem Lett. 2016;7(11):2044-9.